Appl. Phys. B 71, 251–255 (2000) / Digital Object Identifier (DOI) 10.1007/s003400000373

Applied Physics B
Lasers
and Optics

Rapid communication

Characterization of optical and nonlinear properties of periodically-poled $RbTiOAsO_4$ in the mid-infrared range via difference-frequency generation

K. Fradkin-Kashi, A. Arie, P. Urenski, G. Rosenman

Dept. of Electrical Engineering – Physical Electronics, Faculty of Engineering, Tel-Aviv University, Tel-Aviv 69978, Israel
(Fax: 972-36/423-508, E-mail: kerenfr@post.tau.ac.il)

Received: 30 March 2000/Revised version: 9 May 2000/Published online: 30 June 2000 – © Springer-Verlag 2000

Abstract. Tunable mid-infrared coherent radiation (3.25–3.7 μm) is generated by quasi-phase-matched difference frequency generation in a multi-grating periodically-poled $RbTiOAsO_4$ crystal. The spontaneous polarization and coercive field of flux-grown $RbTiOAsO_4$ are determined by polarization switching measurements. The nonlinear interaction enables us to explore the optical and nonlinear properties of this material in the mid-infrared range, where data is scarce. The measurements are used to derive a mid- infrared corrected dispersion equation for n_z in $RbTiOAsO_4$. This equation is in excellent agreement with previously published measurements of nonlinear interactions in periodically-poled $RbTiOAsO_4$. The measured wavelength and temperature bandwidths are ≈ 48 nm cm and ≈ 29 °C cm, respectively. A relatively high temperature tuning slope of the phase-matched idler wavelength, -1.27 nm/°C, is measured. This may be useful for realizing temperature-tuned nonlinear devices.

PACS: 42.70.Mp; 42.79.Nv; 78.20.Ci

During the last few years, practical methods for modulating the nonlinear coefficient in ferroelectric materials by electric field poling have been developed. Quasi-phase-matching (QPM) [1] has been demonstrated with several periodically-poled ferroelectric crystals, including $LiNbO_3$ [2], $KTiOPO_4$ (KTP) [3, 4], $RbTiOAsO_4$ (RTA) [5, 6] and recently also $KTiOAsO_4$ (KTA) [7]. The QPM method is particularly attractive at wavelength regions in which compact and efficient sources are scarce, e.g. in the mid- infrared (mid-IR, 2–10 μm).

Lately, we have explored the nonlinear and optical properties of periodically-poled KTP (PP-KTP) [8] and periodically-poled KTA (PP-KTA) [9] in the mid-IR range by performing QPM difference-frequency generation (DFG) experiments with these crystals, which are known to have a much higher damage threshold compared to periodically-poled $LiNbO_3$ (PP-LN). One of the important characteristics of the alkali metal titanyl arsenate crystals, such as KTA, is that in addition to maintaining most of the valuable properties of KTP, e.g. low coercive field and high damage threshold, they also lack the significant absorption that KTP exhibits around ≈ 3.3 μm. Moreover, they enjoy a longer cutoff wavelength of ≈ 5 μm, compared to ≈ 4 μm in KTP.

Another attractive alkali metal titanyl arsenate crystal is RTA, which also exhibits a long cutoff wavelength, ≈ 5.3 μm. Whereas flux-grown KTP and KTA crystals should be either cooled to a low temperature (≈ 170 K) [4] or pre-treated by chemical indifussion of Rb ions [10], RTA crystals have been poled near room temperature without any pre- treatment [5]. Furthermore, since the poling field increases as the temperature decreases, the electric field required to pole RTA near room temperature is ≈ 2.5 kV/mm [5, 6], less than half of that required for KTP and KTA at 170 K. In addition, the poling field is approximately an order of magnitude lower than that of $LiNbO_3$ [11]. Owing to that, fairly thick samples (≈ 3 mm) have been periodically-poled [12].

Up until now, PP-RTA crystals were only used in optical parametric oscillator (OPO) configurations, from continuous-wave mode [13] and up to ultra-short pulses [14]. In this paper we report, for the first time to the best of our knowledge, DFG of mid-IR coherent radiation using a multi-grating PP-RTA crystal. This nonlinear interaction is used for characterizing the optical and nonlinear properties of PP- RTA in the mid-IR range. One advantage of small signal DFG compared to OPO is that the DFG idler wavelength is fully determined by the choice of the pump and signal wavelengths. Furthermore, unlike in the case of OPO, there is no threshold and the interaction is less dependent on the losses of the interacting waves.

Knowledge about the dispersion in the crystal is required for designing an appropriate modulation period for a specific QPM nonlinear interaction [1]. A design based on an inaccurate dispersion equation could result in significant mismatch and therefore less than optimum frequency conversion efficiency. Alternatively, it may cause constraints on the operating conditions, e.g. crystal temperature, pump and signal wavelengths, etc., in order to achieve phase-matching.

Table 1. Grating periods in experiments of nonlinear interactions with PP-RTA crystals at room temperature, and deviations of periods calculated according to dispersion equations from the actual values. The effect of focusing was neglected in this calculation

Experimental data			Deviation of calculated period from experimental period (%)			
Nonlinear interaction	Ref.	Grating period (μm)	Ref. [15]	Ref. [16]	Ref. [17]	This work
SHG 0.873 μm ⇒ 0.4365 μm	5	4.2	0.59	0.61	17.6	0.02
OPO 1.0644 μm ⇒ 1.577 μm, 3.275 μm	12	40.2	6.22	0.8	93.49	0.49
OPO 0.84 μm ⇒ 1.18 μm, 2.915 μm	13	30	2.78	1.58	37.17	1.52
OPO 0.835 μm ⇒ 1.07 μm, 3.802 μm	18	30	4.21	1.487	61.39	0.12

Only few dispersion equations for RTA appear in the literature [15–17]. In a variety of recently published experiments with PP-RTA, discrepancies between the actual grating periods and the calculated ones have been observed. Table 1 gives several examples [5, 12, 13, 18] for the grating periods used in experiments with PP-RTA at room temperature. The deviations of the calculated periods are given for the three existing dispersion equations. It is clearly seen that even with the most accurate dispersion equation [16], deviations of up to $\approx 1.5\%$ are still present. Such deviations have a profound effect on the performance of nonlinear devices. For example, Fig. 1 shows the measured tuning curve of a PP-RTA based OPO (squares) [18] together with the theoretically calculated tuning curve (dashed line) based on the dispersion equation of [16]. It can be seen that for idler wavelengths (mid-IR range) there is a discrepancy of up to 1 μm ($\approx 20\%$) between the measurements and the calculation. Moreover, even for the signal wavelengths (near infrared) there is a slight deviation.

Previous measurements of the refractive indices of RTA were performed using the critical angle of refraction [15], minimum deviation [16] and variable angle spectroscopy ellipsometry [17] methods. In this paper we use QPM nonlinear interactions in PP-RTA in order to derive a mid-IR corrected dispersion equation of n_z. This method has already been successfully used for the derivation of mid-IR corrected dispersion equations of n_z in other nonlinear crystals from the same family, namely KTP [8] and KTA [9]. It also provided accurate results for $LiNbO_3$ [19].

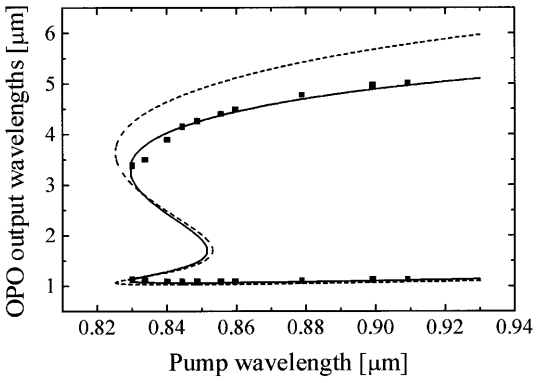

Fig. 1. Tuning curve of a PP-RTA-based picosecond OPO. Experimental results taken from [18] (*squares*); the *dashed curve* is calculated using dispersion equation of [16]; *solid curve* is calculated using the newly derived dispersion equation, (2)

1 Dielectric spectroscopy and polarization switching of $RbTiOAsO_4$

The 0.5-mm thick flux-grown RTA crystal (grown by Crystal Associates) was poled using the electric-field poling technique [20]. In order to find appropriate experimental conditions for the fabrication of the domain grating structure with minimal domain broadening effect, dielectric spectroscopy and dc conductivity of RTA samples were studied [20]. The dielectric permittivity was measured at room temperature for the RTA sample. The real part of the relative permittivity, ε', was ≈ 50 at 1 kHz and the dielectric loss, $\tan\delta$, was 0.4. Such properties provide direct evidence for the relaxation process in RTA crystals at room temperature. This fact is supported by measurements of a room temperature dc conductivity of $5 \times 10^{-9}\,\Omega^{-1}\mathrm{cm}^{-1}$, as well as an unsaturated hysteresis loop exhibiting remnant dielectric leakage. Cooling the RTA crystal to 240 K led to a decrease in the dc conductivity by two orders of magnitude. It also led to a strong suppression of the dielectric dispersion. The hysteresis loop measured at 240 K (see Fig. 2) was completely saturated and the derived spontaneous polarization P_s was $33\,\mu\mathrm{C/cm}^2$, which is close to the previously reported value for RTA of $40\,\mu\mathrm{C/cm}^2$ [6]. The hysteresis loop exhibited asymmetry with respect to the applied electric field, with coercive fields of $E_C^- = -4.15\,\mathrm{kV/mm}$ and $E_C^+ = 2.7\,\mathrm{kV/mm}$.

The pyroelectric effect was used to monitor the quality of the fabricated domain structure. In a periodically-poled crystal with 50% duty cycle the pyroelectric effect should vanish. Our measurements showed that the value of the pyroelectric coefficient of a monodomain RTA crystal is $4\,\mathrm{nC\,cm^{-2}K^{-1}}$. Monitoring in situ the electrical poling process using the pyroelectric current measurements allowed us to fabricate RTA

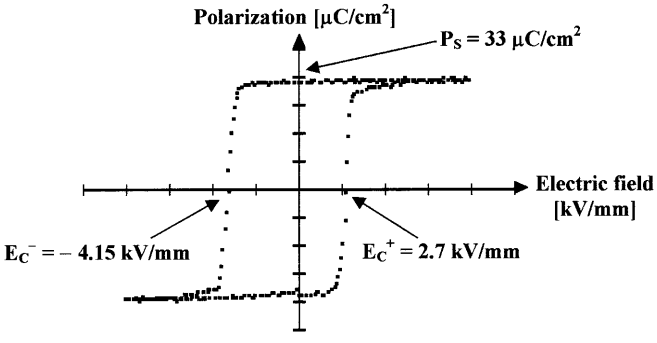

Fig. 2. Dielectric hysteresis loop of RTA, measured at 240 K

samples with a fairly homogeneous periodically-poled domain structure and good quality. Three gratings with periods of 39.6, 39.9 and 40.2 μm were poled on the 3-mm long RTA crystal.

2 Difference-frequency generation in periodically-poled $RbTiOAsO_4$

The DFG experimental setup is shown in Fig. 3. It consists of two compact laser sources that lase in a single longitudinal and spatial (TEM_{00}) mode: a diode-pumped Nd:YAG laser at 1064.4 nm (Lightwave Electronics model 122) and an external cavity tunable diode laser (New-Focus model 6328-H, tunable between 1486 nm and 1584 nm). The beams of the pump and signal lasers are combined collinearly using a dichroic beamsplitter and are focused into the uncoated multi-grating PP-RTA crystal.

In our experiment the mixing process occurs through the largest nonlinear coefficient in RTA, $d_{33} = 15.8\,\mathrm{pm/V} \pm 20\%$ [15]. Mid-IR radiation at wavelengths between 3.25 and 3.7 μm is generated in the PP-RTA crystal. The radiation is focused onto a 1-mm-diameter liquid-nitrogen-cooled HgCdTe detector (Fermionics model PV-6-1), which exhibits a noise-equivalent power of $\approx 1\,\mathrm{pW}/\sqrt{\mathrm{Hz}}$. A tilted uncoated Germanium window is used to block the pump and signal beams from entering the detector. The signal beam is chopped at a rate of 1.5 kHz, and the idler is detected with a lock-in amplifier. The wavelengths of the pump and signal lasers are measured using a wavemeter (Burleigh WA-20).

With 131.5 mW Nd:YAG power at 1064.4 nm and 17.5 mW of diode power at 1532.3 nm incident on the uncoated mixing crystal having a period of 39.6 μm, a maximum idler power of 16.8 nW is measured at the detector. Taking into account the transmission of all uncoated components in the setup, this measured infrared power indicates a normalized internal conversion efficiency of 0.004%/(W cm).

The theoretical expression for DFG efficiency for the case of two Gaussian beams with a joint waist location at the middle of the crystal is [21] (SI units):

$$\eta = \frac{P_\mathrm{i}}{P_\mathrm{p} P_\mathrm{s} l} = \frac{4\omega_\mathrm{i}^2 k_\mathrm{s} d_\mathrm{eff}^2 h(\xi, \mu, \Delta k)}{\pi n_\mathrm{p} n_\mathrm{s} n_\mathrm{i} \varepsilon_0 c^3 (1+\mu)} \tag{1}$$

where ω_i is the idler angular frequency; k_s is the signal wavevector; d_eff is the effective nonlinear coefficient; n_p, n_s and n_i are the refractive indices for the pump, signal and idler wavelengths respectively; ε_0 and c are the permittivity and the speed of light in free space, respectively; μ is the ratio between the signal and pump wavevectors; ξ is the ratio between the crystal length and the confocal parameter; Δk is the wavevector mismatch and $h(\xi, \mu, \Delta k)$ is the focusing function, which assumes equal confocal parameters for the pump and signal beams. Unfortunately, the two beams had different confocal parameters, as well as non-coinciding waist positions (≈ 1.85 mm distance between the waists). For DFG interactions with unequal confocal parameters, the focusing function, h, is given in [22], nevertheless it still assumes a joint waist position in the middle of the crystal. Note that because of a slightly different definition, one has to multiply the focusing function of [22] by a factor of 2 before substituting it in (1). In our experiment the profile of both beams was slightly elliptic (average beam radii: $\omega_{0\mathrm{p}} \approx 21$ μm and $\omega_{0\mathrm{s}} \approx 42$ μm) and $\mu \approx 0.69$. Assuming $d_\mathrm{eff} = (2/\pi) d_{33} \approx 8.2\,\mathrm{pm/V} \pm 20\%$ (taking into account Miller's delta), the theoretical conversion efficiency should be between 0.012 and 0.026%/(W cm). The effects of the ellipticity of the beams and their non-coinciding waist positions were evaluated numerically and led to a total reduction in the calculated efficiency of ≈ 11%. The remaining discrepancy with respect to the measured efficiency may be explained by other effects that are more difficult to quantify: the deviation of the laser beams from ideal TEM_{00} Gaussian beams and possible imperfections of the periodically-poled crystal.

The DFG power as a function of the generated idler wavelength at room temperature is shown in Fig. 4 for three gratings with periods 39.6, 39.9 and 40.2 μm. The full width at half maximum for the idler wavelength is ≈ 160 nm. Taking into account the length of the crystal, ≈ 3 mm, this indicates a normalized bandwidth of 48 nm cm. The asymmetry of the measured efficiency as a function of the idler wavelength is caused by the focused Gaussian beams [22]. In contrast to the case of plane wave interactions, the highest efficiency is obtained at a nonzero wavevector mismatch. For the conditions of our experiment, the highest efficiency is obtained with a theoretically calculated wavevector mismatch of $\approx 530\,\mathrm{m}^{-1}$ [22].

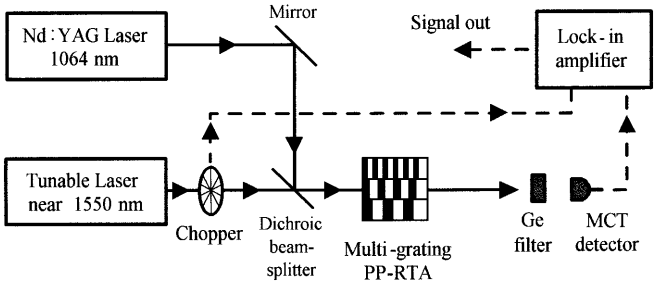

Fig. 3. Experimental setup for DFG of mid-IR radiation in a multi-grating PP-RTA crystal

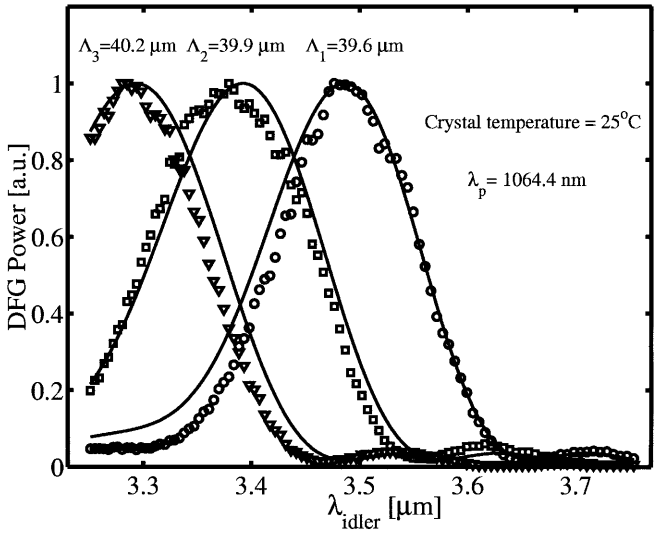

Fig. 4. Normalized DFG power as a function of the generated wavelength, as measured with a multi-grating PP-RTA crystal (grating periods: 39.6 μm, *circles*; 39.9 μm, *squares*; 40.2 μm, *triangles*). *Solid curves* are calculated using (2)

We also measured the DFG power as a function of the crystal temperature. For the 39.6-μm grating period, and with signal wavelengths of 1538.1 nm and 1542.1 nm, the peak efficiency was measured at a temperature of ≈ 49 °C and ≈ 64 °C, respectively. The derived tuning slope for the idler wavelength, −1.27 nm/°C, is higher than that measured for PP-KTP, −0.5 nm/°C [8], and for PP-KTA, −0.94 nm/°C [9], and is almost as high as the calculated tuning slope for PP-LN, −1.5 nm/°C [19]. The large temperature-tuning slope of PP-RTA can be advantageous for realizing tunable nonlinear devices, e.g. temperature-tuned OPO [23], but may also require a temperature stabilization of the crystal for long-term wavelength stability. We have also measured a temperature full width at half maximum of ≈ 97 °C. This corresponds to a normalized bandwidth of ≈ 29 °C cm, similar to the calculated bandwidth for PP-LN [19].

3 Derivation of mid-infrared corrected dispersion equation for the *Z* direction in $RbTiOAsO_4$

Of the three existing dispersion equations for RTA, [16] gives the closest prediction of the phase-matched idler wavelengths in our experiment. However, the predicted idler wavelengths still deviate by up to 3.1% from the actual measured phase-matched wavelengths. With a pump wavelength of 1064.446 nm and the crystal held at room temperature, idler wavelengths of 3.486, 3.378 and 3.288 μm were generated with grating periods of 39.6, 39.9 and 40.2 μm, respectively. We used these measurements to derive a dispersion equation. The general form of the refractive index in the *Z* direction of RTA is:

$$n_z^2 = A + \frac{B}{1-\left(C/\lambda\right)^2} + \frac{D}{1-\left(E/\lambda\right)^2} - F\lambda^2. \qquad (2)$$

Initially we attempted to fit our experimental data in the 1.53–3.48 μm range, as well as measurements of Fenimore et al. [16] in the 0.8–1.3 μm range, using a reduced form of (2) with a single pole in the ultraviolet range, as was used in [15, 16]. The best fit we achieved with this form still had a deviation of up to 1.3% in predicting the phase-matched idler wavelengths. Considering the large absorption in RTA for wavelengths longer than 5.3 μm, we have added a second pole in the mid-IR region. This approach has proven to give improved accuracy for KTP [8] and KTA [9]. The addition of the second pole is also justified by statistical calculations using the F-test [24], giving a confidence level better than 99.9%. By doing so, we improved the accuracy of the predicted phase- matched idler wavelengths to 0.46%. The parameters of this fit are as follows: $A = 2.182064$; $B = 1.307519$; $C = 0.228244$; $D = 0.354743$; $E = 9.010959$; $F = 0.008921$; where λ is given in μm. The new dispersion equation was used to calculate the expected phase-matching curves at room temperature. These curves appear in Fig. 4 together with the measured data, and it can be seen that in addition to predicting correctly the location of the central peak, they also fit the first sideband. The nonzero wavevector mismatch for tightly focused Gaussian beams [22] was taken into account in the calculation of the dispersion equation coefficients. The wavevector mismatch for the experimentally measured wavelengths and using the refractive indices calculated with (2) was $\approx 570\,\mathrm{m}^{-1}$, which is indeed close to the theoretical value for the focussing conditions used in the experiment, $\approx 530\,\mathrm{m}^{-1}$. The calculated bandwidth of ≈ 168 nm is in good agreement with the measured bandwidth of ≈ 160 nm, thus indicating that the periodically-poled length is approximately the entire 3-mm physical length of the crystal.

The accuracy of the dispersion equation derived here, (2), in predicting the grating periods for published measurements with PP-RTA crystals is shown in Table 1. With this equation, the deviation of the calculated grating period from the experimental period was significantly reduced, in some cases by more than an order of magnitude. In Fig. 1, the theoretically calculated tuning curve based on (2) (solid line) is shown together with the measurements (squares) and the calculated tuning curve based in [16] (dashed line). The curve based on (2) shows excellent agreement with the measured results. While the calculation based on [16] has an average deviation of 17.9% in the idler wavelength (mid-IR range), (2) reduced this deviation significantly to 2.3%. Moreover, it also shows a slight improvement in the near-IR range, reducing the average deviation in the signal wavelength from 3.8% to only 0.6%. These comparisons indicate that the dispersion equation derived here is valid not only for the specific PP-RTA sample that was used in our experiment, but also provides improved accuracy for different samples of this material.

4 Conclusions

We have explored the optical and nonlinear properties of RTA in the mid-IR spectral range by difference frequency generation in PP-RTA. We have obtained a mid-IR corrected dispersion equation with improved accuracy, and measured the temperature and wavelength tuning bandwidths. The temperature tuning slope was found to be much larger than that of other isomorphs of the KTP family and comparable with that of PP-LN. A widely-tuned mid-IR coherent source (3.25–3.7 μm) was produced and can be readily applied for sensitive spectroscopic measurements of gases [9]. Furthermore, the possibility of attaining wide aperture PP-RTA crystals, as well as the high damage threshold, can be useful for high power frequency conversion devices, particularly in the mid-IR range.

Acknowledgements. This work was supported by a grant from the ministry of science, culture and sport of Israel, and by the German–Israeli foundation for scientific research and development.

References

1. J.A. Armstrong, N. Bloembergen, J. Ducuing, P.S. Pershan: Phys. Rev. **127**, 1918 (1962)
2. M. Yamada, N. Nada, M. Saitoh, K. Watanabe: Appl. Phys. Lett. **62**, 435 (1993)
3. Q. Chen, W.P. Risk: Electron. Lett. **30**, 1516 (1994)
4. G. Rosenman, A. Skliar, D. Eger, M. Oron, M. Katz: Appl. Phys. Lett. **73**, 3650 (1998)
5. H. Karlsson, F. Laurell, P. Henriksson, G. Arvidsson: Electron. Lett. **32**, 556 (1996)

6. Z.W. Hu, P.A. Thomas, J. Webjorn, G.M. Loiacono: J. Phys. D: Appl. Phys. **29**, 1681 (1996)
7. G. Rosenman, A. Skliar, Y. Findling, P. Urenski, A. Englander, P.A. Thomas, Z.W. Hu: J. Phys. D: Appl. Phys. **32**, L49 (1999)
8. K. Fradkin, A. Arie, A. Skliar, G. Rosenman: Appl. Phys. Lett. **74**, 914 (1999)
9. K. Fradkin-Kashi, A. Arie, P. Urenski, G. Rosenman: Opt. Lett. **25**, 743 (2000)
10. H. Karlsson, F. Laurell: Appl. Phys. Lett. **71**, 3474 (1997)
11. L.E. Myers, R.C. Eckardt, M.M. Fejer, R.L. Byer, W.R. Bosenberg, J.W. Pierce: J. Opt. Soc. Am. B **12**, 2102 (1995)
12. H. Karlsson, M. Olson, G. Arvidsson, F. Laurell, U. Bader, A. Borsutzky, R. Wallenstein, S. Wickstrom, M. Gustafsson: Opt. Lett. **24**, 330 (1999)
13. T.J. Edwards, G.A. Turnbull, M.H. Dunn, M. Ebrahimzadeh, H. Karlsson, G. Arvidsson, F. Laurell: Opt. Lett. **23**, 837 (1998)
14. P. Loza-Alvarez, D.T. Reid, M. Ebrahimzadeh, W. Sibbett, H. Karlsson, P. Henriksson, G. Arrvidsson, F. Laurell: Appl. Phys. B **68**, 177 (1999)
15. L.K. Cheng, L.T. Cheng, J. Galperin, P.A. Morris Hotsenpiller, J.D. Bierlein: J. Crystal Growth **137**, 107 (1994)
16. D.L. Fenimore, K.L. Schepler, D. Zelmon, S. Kuck, U.B. Ramabadran, P. von Richter, D. Small: J. Opt. Soc. Am. B **13**, 1935 (1996)
17. C.-S. Tu, R.S. Katiyar, V.H. Schmidt, R. Guo, A.S. Bhalla: Phys. Rev. B **59**, 251 (1999)
18. G.T. Kennedy, D.T. Reid, A. Miller, M. Ebrahimzadeh, H. Karlsson, G. Arvidsson, F. Laurell: Opt. Lett. **23**, 503 (1998)
19. D.H. Jundt: Opt. Lett. **22**, 1553 (1997)
20. G. Rosenman, A. Arie, A. Skliar: Ferroelectr. Rev. **1**, 263 (1999)
21. T.B. Chu, M. Broyer: J. Phys. **46**, 523 (1985)
22. S. Guha, F.-J. Wu, J. Falk: IEEE J. Quantum Electron. **QE-18**, 907 (1982)
23. A. Garashi, A. Arie, A. Skliar, G. Rosenman: Opt. Lett. **23**, 1739 (1998)
24. C. Daniel, F.S. Wood: *Fitting Equations to Data: Computer Analysis of Multifactor Data for scientists and Engineers* (John Wiley & Sons, Inc. Canada 1971) Chapt. 6, 8